



Universiteit  
Leiden  
The Netherlands

## **Molecular imaging of pancreatic and rectal cancer: on a path towards optimized detection and response prediction**

Vuijk, F.A.

### **Citation**

Vuijk, F. A. (2024, January 10). *Molecular imaging of pancreatic and rectal cancer: on a path towards optimized detection and response prediction*. Retrieved from <https://hdl.handle.net/1887/3677368>

Version: Publisher's Version

License: [Licence agreement concerning inclusion of doctoral thesis in the Institutional Repository of the University of Leiden](#)

Downloaded from: <https://hdl.handle.net/1887/3677368>

**Note:** To cite this publication please use the final published version (if applicable).

Baseline and early digital [<sup>18</sup>F]FDG PET/CT and multiparametric MRI contain promising features to predict response to neoadjuvant therapy in locally advanced rectal cancer patients: a pilot study.

F.A. Vuijk, S. Feshtali Shahbazi, W.A. Noortman, F.H.P. van Velden, P. Dibbets-Schneider, A.W.K.S. Marinelli, P.A. Neijenhuis, R. Schmitz, E. Ghariq, L.A. Velema, F.P. Peters, F. Smit, K.C.M.J. Peeters, J.S.D. Temmink, A.S.L.P. Crobach, H. Putter, A.L. Vahrmeijer<sup>a</sup>, D.E. Hilling and L.F. de Geus-Oei.

*Nuclear Medicine Communications 2023*



## ABSTRACT

In this pilot study we investigated the feasibility of response prediction using digital [<sup>18</sup>F]FDG PET/CT and multiparametric MRI before, during and after neoadjuvant chemoradiation therapy in locally advanced rectal cancer patients, and aimed to select the most promising imaging modalities and timepoints for further investigation in a larger trial. Rectal cancer patients scheduled to undergo neoadjuvant chemoradiation therapy were prospectively included in this trial, and underwent multiparametric MRI and [<sup>18</sup>F]FDG PET/CT before-, 2 weeks into- and 6-8 weeks after chemoradiation therapy. Two groups were created based on pathological tumor regression grade, i.e. good responders (TRG1-2) and poor responders (TRG3-5). Using binary logistic regression analysis with a cut-off value of  $p \leq 0.2$ , promising predictive features for response were selected. Nineteen patients were included. Of these, 5 were good responders and 14 poor responders. Patient characteristics of these groups were similar at baseline. Fifty-seven features were extracted, of which 13 were found to be promising predictors of response. Baseline (T2: volume, DWI: ADC mean, DWI: difference entropy), early response (T2: volume change, DWI: ADC mean change) and end-of-treatment pre-surgical evaluation MRI (T2: grey level non-uniformity, DWI: inverse difference normalized, DWI: grey level non-uniformity normalized) as well as baseline (MTV, TLG) and early response PET/CT ( $\Delta SUV_{max}$ ,  $\Delta SUL_{peak}$ ) were promising features. Both multiparametric MRI and [<sup>18</sup>F]FDG PET/CT contain promising imaging features to predict response to nCRT in LARC patients. A future larger trial should investigate baseline, early response and end-of-treatment pre-surgical evaluation MRI and baseline and early response PET/CT.

## INTRODUCTION

Patients diagnosed with locally advanced rectal cancer (LARC) are currently treated with neoadjuvant chemoradiotherapy (nCRT), prior to surgical resection. The goal of nCRT is to downsize and downstage the rectal cancer, thereby improving the rate of complete resections and lowering the risk of local recurrence<sup>1</sup>. The majority of patients has a partial tumor response after nCRT<sup>1</sup>, while in 15-20% this even results in a pathological complete response (pCR) of all tumor tissue<sup>1,2</sup>. Most recently, results from the RAPIDO trial demonstrate even higher rates of pCR (28%) after neoadjuvant short course radiotherapy followed by chemotherapy<sup>3</sup>. Unfortunately, not all patients respond well to nCRT, but the exact number of non-responders is uncertain<sup>4</sup>.

According to current guidelines, treatment stratification and response assessment is performed using magnetic resonance imaging (MRI) and in selected cases, rectoscopy<sup>5</sup>. MRI features include the TNM stage, extramural vascular invasion (EMVI) and tumor distance to the mesorectal fascia<sup>6</sup>. Unfortunately, current imaging modalities are unable to predict response to nCRT accurately. In recent years, the Watch-and-Wait strategy has been implemented for patients with a clinical complete response (cCR) after neoadjuvant therapy, with excellent long-term outcome<sup>1,7</sup>. By means of improved stratification before or early after onset of nCRT, precise selection of patients might be possible. In patients predicted to respond well, the (watchful) waiting period before surgery could be prolonged, possibly increasing the rate of cCR. Accurate identification of cCR patients can prevent futile surgery and its associated morbidity and mortality<sup>8</sup>. In patients with a predicted poor response, unbeneficial continuation of nCRT, therapy related toxicity and unwanted delay in initiation of a potentially effective treatment could be avoided.

Currently, 2-[<sup>18</sup>F]fluoro-2-deoxy-D-glucose ([<sup>18</sup>F]FDG) positron emission tomography combined with computed tomography (PET/CT) is advised in the national guideline for the detection of recurrence of rectal cancer in case of increased carcinoembryonic antigen (CEA) levels<sup>9</sup>. Many MRI and [<sup>18</sup>F]FDG PET/CT features have been investigated separately to predict response to nCRT before or early after onset of nCRT<sup>10-21</sup>. The combination of both modalities could possibly have complimentary value to predict response. Available data in the literature are insufficient to evaluate this approach, and no studies have investigated the application of digital PET/CT in this field<sup>13,16,19</sup>. Owing to its increased energy resolution and time-of-flight performance, digital PET/CT has the potential to improve quantification of small or heterogeneous tumors and thereby provide more accurate metabolic information on tumor response, and might (in combination with multiparametric MRI) facilitate improved response prediction to nCRT.

In this pilot study we investigate the feasibility of response prediction using digital [<sup>18</sup>F]

FDG PET/CT and multiparametric MRI before, during and after nCRT in LARC patients, and aim to determine the most promising imaging modalities and timepoints for further investigation.

## MATERIALS AND METHODS

### Patient population

A multicenter, non-randomized prospective study was performed in patients admitted to the Leiden University Medical Center (LUMC, n=8), Haaglanden Medical Center (n=6), Alrijne Hospital Leiderdorp (n=4) and Groene Hart Hospital (n=1), diagnosed with (biopsy proven) LARC and treated according to national guidelines. Eligible patients were selected at multidisciplinary meetings, and asked for participation during their outpatient clinic visit. Treatment consisted of nCRT (25x2 Gy combined with 825 mg/m<sup>2</sup> bid capecitabine 5 days per week), followed by reevaluation after 6-8 weeks. Surgery followed within 4-6 weeks after reevaluation. In case of a near complete response, reevaluation was repeated after 6-8 weeks. In case of cCR, follow up was initiated according to the Watch-and-Wait protocol<sup>7</sup>. The study was conducted in concordance with the Declaration of Helsinki, and was approved by the Leiden-Den Haag-Delft medical ethics review board and the local boards of participating centers. All subjects provided written informed consent. The study was registered in the Netherlands Trial Register (identification number NL-756). Including standard of care imaging (rectoscopy, MRI scan of abdomen and CT scan of the chest and abdomen), all patients underwent [<sup>18</sup>F]FDG PET/CT and multiparametric MRI before nCRT, 10-14 days after nCRT onset (early response evaluation), and 6-8 weeks after the last treatment (end-of-treatment pre-surgical evaluation).

### Data acquisition and image reconstruction

All digital [<sup>18</sup>F]FDG PET/CT scans of the lower abdomen were acquired on the same scanner, a Vereos PET/CT (Philips Healthcare, Best, the Netherlands). All acquisitions and reconstructions were in accordance with EANM guidelines for tumor PET imaging version 2.0<sup>22</sup>. Prior to PET/CT scanning, patients fasted for 6 hours and were prehydrated using 1 L of water. [<sup>18</sup>F]FDG was dosed using the quadratic formula:  $379 \text{ (MBq}\cdot\text{min}\cdot\text{bed}^{-1}\cdot\text{kg}^{-2}) \times (\text{patient weight (kg)/75})^2 / \text{emission acquisition duration per bed position (min}\cdot\text{bed}^{-1})$  with a factor of  $379 \text{ MBq}\cdot\text{min}\cdot\text{bed}^{-1}\cdot\text{kg}^{-2}$ . Patients received 20 mg intravenous furosemide 15 min post injection. Patients underwent a low-dose CT scan for attenuation correction 60 (55-65) min post injection (120 kV, 35 mA<sub>eff</sub>), followed by a PET scan of 5 minutes per bed position. Reconstructed PET images had a voxel size 4x4x4 mm. Multiparametric MRI of the lower abdomen was made on various systems, and included T2- and diffusion weighted imaging (DWI) sequences. Patients underwent bowel preparation using a 5 mL Microlax® enema three hours before imaging (Johnson and Johnson, New Brunswick,

New Jersey, United States). Further details are described in **Supplemental Table 1**.

### Quantitative image analysis

MRI assessment was performed by a board-certified abdominal radiologist (S.F.S., 11 years of experience), using Sectra IDS7 software (version 21.2; Sectra AB, Linköping, Sweden). Apparent diffusion coefficient (ADC) values were calculated from the DWI image. Volumes of interest (VOIs) were drawn manually (F.V. under supervision of S.F.S.) to include the primary tumor on the DWI and T2 maps. Various quantitative features were extracted using 3DSlicer (version 4.11)<sup>23</sup> and PyRadiomics (version 3.0) that was running in Python (version 3.7; Python Software Foundation, Wilmington, Delaware)<sup>24</sup>. First, following the methodology of Schurink *et al.*<sup>19</sup>, the following features were extracted from the VOIs: T2 mesh volume, T2 entropy, DWI mesh volume, mean ADC, ADC entropy, and their respective response indices (RI). Second, to allow full comparison to the results from Schurink *et al.*<sup>19,20</sup> and following recent promising results from Delli Pizzi *et al.*<sup>25</sup>, 105 radiomic features were extracted from the T2 baseline images for additional radiomic analysis: shape (14), first order (18), grey level cooccurrence matrix (22), grey level run length matrix (16), grey level size zone matrix (16), grey level dependence matrix (14) and neighboring grey tone difference matrix (5) features. Images were interpolated to isotropic voxels of 2.00x2.00x2.00 mm<sup>3</sup> using B-spline interpolation, with grids aligned by the input origin and only covering the VOI. Both T2 and DWI images were normalized to a mean of 300 and a standard deviation of 100, allowing comparison of the relative gray values between patients<sup>26</sup>. Features were extracted using a fixed bin size, which was determined in such a way that most VOIs contained between 30-130 bins. This resulted in a bin size of 5 and 15 for T2 and DWI images, respectively.

PET/CT assessment was performed by a board-certified nuclear medicine physician (L.G., 25 years of experience), using Sectra IDS7 software (version 21.2; Sectra AB, Linköping, Sweden). VOIs were automatically delineated with an isocontour threshold of 50% of the maximal standardized uptake value (SUV<sub>max</sub>) using IntelliSpace Portal (version 9.0; Koninklijke Philips N.V., Amsterdam, the Netherlands). The following features were included in the analysis with their corresponding RI based on the following articles. Joye *et al.* pooled data from 25 studies investigating [<sup>18</sup>F]FDG PET/CT and found the following features to be promising predictors for response<sup>17</sup>: the SUV<sub>max</sub> post therapy, RI of the SUV<sub>max</sub>, the metabolic tumor volume (MTV, obtained using a SUL<sub>peak</sub> threshold of 50%) and total lesion glycolysis (TLG, SUV<sub>mean</sub> x MTV). All features were body weighted, except SUL<sub>peak</sub> which was weighted using the lean body mass following the methodology described in PERCIST 1.0 and by O *et al.*<sup>27</sup>. They advise the use of SUL<sub>peak</sub> as exploratory data when the liver is not present in all scans. No radiomic feature analysis was performed on data from [<sup>18</sup>F]FDG PET/CT, as this has not been described in literature before.

## Pathology

Pathological assessment of the resection specimen was performed according to the Dutch national guidelines<sup>9</sup>. In addition to this, the extent of tumor regression was evaluated according to Mandard's Tumor Regression Grade (TRG) by the local board certified pathologist<sup>28</sup>. Mandard's TRG classifies response to given therapy in 5 classes based on the amount of vital tumor cells and extent of therapy induced fibrosis. When classified TRG 1, no residual tumor cells were seen, and the patient is considered to have a pathologic complete response (pCR). A regrowth free survival time of >6 months was considered a surrogate endpoint for TRG1 in patients with a cCR in Watch-and-Wait follow up.

## Statistical analysis

Statistical analysis was performed using SPSS (version 25; IBM SPSS, Inc., Chicago, USA) and R (version 3.6.0; R Foundation for Statistical Computing, Vienna, Austria). For statistical analysis, patients were divided into two groups based on the pathological TRG or regrowth free follow up in case of Watch-and-Wait: good responders (TRG1-2) and poor responders (TRG 3-5). Descriptive data were displayed as mean  $\pm$  standard deviation or median (interquartile range), depending on the distribution of data. Non-parametric data were compared using the Mann Whitney U test, whereas parametric data were compared using a T-test. Results were considered significant when  $p < 0.05$ . Promising imaging features were selected using binary logistic regression, after dividing through their respective standard deviation. Due to the small sample size and large amount of tested features, MRI and PET/CT features were considered promising when a  $p$ -value  $\leq 0.2$  was reached.

Unsupervised radiomic feature selection using redundancy filtering and factor analysis was performed using FMradio (Factor Modeling for Radiomics Data, package version 1.1.1; Amsterdam UMC, Amsterdam, the Netherlands), developed for R (version 3.6.0; R Foundation for Statistical Computing, Vienna, Austria)<sup>29</sup>. The large feature dimensionality compared to the small sample size might result in overfitting and deteriorates the generalizability of the radiomic model. Therefore, one feature was selected for every ten subjects<sup>30</sup>. Features were scaled (centered around 0, variance of 1) to avoid that features with the largest value would dominate the analysis. Redundancy filtering on Pearson correlation matrix was performed with a threshold of  $\tau = 0.95$  and from each group one feature was retained. Factor analysis of the redundancy filtered correlation matrix was performed and two factors (19 patients) were selected per sequence and time point. The sampling adequacy of the model was determined by the Kaiser-Meier-Olkin (KMO) measure, which had to be between 0.9 and 1.0. The features with the highest loading on the factors were selected.

## RESULTS

Nineteen patients were included in the period between July 2018 and March 2020. All patients completed chemoradiotherapy, and all but one underwent surgery after an average of  $14.1 \pm 6.6$  weeks (one cCR patient in Watch-and-Wait). All but one patient completed all 6 imaging studies: in one patient the final [<sup>18</sup>F]FDG PET/CT was not performed due to logistical problems. Sixteen men and three women were included in this study with a median age of 63.1 (56.3-67.0) years old. The median follow up time was 11.6 (9.0-17.1) months. No recurrent disease was found. One patient had a cCR without regrowth during follow up, four patients had a pTRG1, 9 pTRG3, 4 pTRG4 and 1 pTRG5. Based on the pTRG, 5 patients (26.3%) were good responders, 14 (73.7%) were poor responders. There were no significant differences at baseline between groups regarding age, sex, cT stage, cN stage, EMVI, and tumor differentiation, as summarized in **Table 1**.

**TABLE 1. Patient and tumor characteristics at baseline.** Table shows difference between the good and poor response group at baseline with corresponding  $p$ -value.

		Good response (n=5)	Poor response (n=14)	p-value
Age (years)	Mean $\pm$ SD	63.6 $\pm$ 11.08	62.9 $\pm$ 6.12	0.273
Gender	Male	4	12	0.770
	Female	1	2	
cT	2	1	0	0.363
	3	3	10	
	4	1	4	
cN	0	1	2	1.00
	1	0	1	
	2	4	11	
EMVI	Yes	0	3	0.565
	No	5	11	
	Missing	0	0	
Differentiation (biopsy)	Well/moderate	3	13	0.071
	Poor	1	0	
	Missing	1	1	

Abbreviations: SD, standard deviation; cT, clinical tumor stage on routine staging MRI; cN, clinical nodal stage on routine staging MRI; EMVI, extramural vascular invasion; IQR, interquartile range. \* Significant difference between groups ( $p < 0.05$ ).

## Quantitative features

A total of 57 quantitative features were extracted. Redundancy filtering and factor analysis of the radiomic feature sets was performed and KMOs were excellent ( $> 0.96$ ). The features corresponding best with the two factors per sequence and timepoint were included in the analysis.

Using binary logistic regression analysis with predefined cut off value of  $p \leq 0.2$ , 13 features were found to be promising predictors of response. At baseline imaging, 3 MRI and 2 PET/CT features were found to be promising. At early response evaluation, no promising features were found. However, 2 MRI and 2 PET/CT early response evaluation to baseline response index features were found to be promising. At end-of-treatment pre-surgical evaluation, 3 MRI and 1 PET/CT feature were found to be promising, but no response index features were promising.

These results are shown in more detail in the forest plot in **Figure 1**, which displays all features with their respective odds ratio and confidence interval. It shows numerous features to have preferable odds ratios. However, only 13 have a  $p \leq 0.2$ . Detailed results from binary logistic regression analysis are displayed in **Table 2**. **Figure 2 and 3** present examples of a good and poor responder on sequential multimodality imaging.

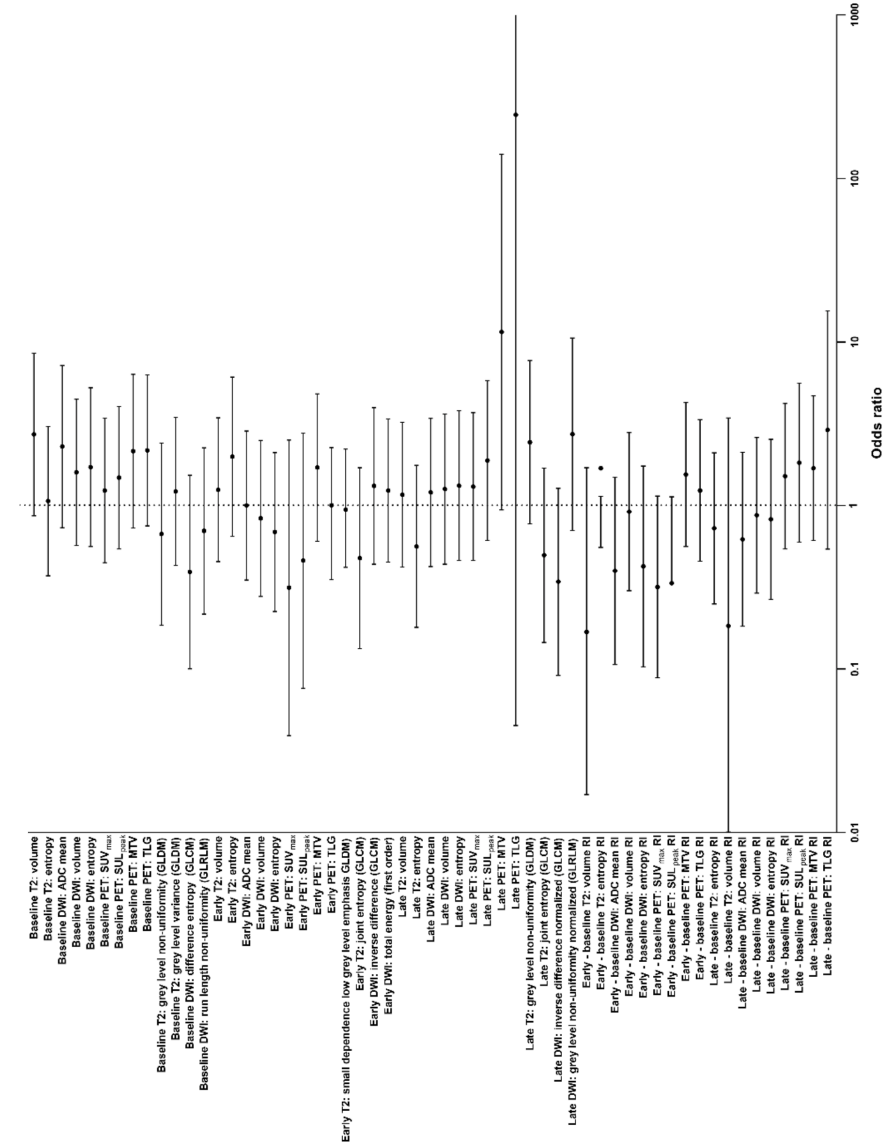


**FIGURE 1. Forrest plot of investigated features.** Figure shows odds ratio for TRG1-2 with 95% confidence intervals from binary logistical regression analyses on logarithmic scale (x-axis). Abbreviations: SUV<sub>max</sub>: maximum standardized uptake value; SUV<sub>peak</sub>: peak standardized uptake value corrected for lean body mass; MTV: metabolic tumor volume; TLG, total lesion glycolysis; T2 volume, tumor volume on T2 series; T2 entropy, tumor entropy on T2 series; DWI volume, tumor volume on diffusion weighted imaging series; ADC mean, mean apparent diffusion coefficient; DWI entropy, tumor entropy on diffusion weighted imaging series; GLCM: grey level cooccurrence matrix, GLDM: grey level dependence matrix, GLRLM: grey level run length matrix, RI, response index (change over time).

**TABLE 2. Binary logistical regression analysis of MRI and PET/CT features for prediction of response.**

Table shows regression coefficient, odds ratios with confidence intervals and p-values. Abbreviations: SUV<sub>max</sub>, maximum standardized uptake value; SUL<sub>peak</sub>, peak standardized uptake value corrected for lean body mass; MTV, metabolic tumor volume; TLG, total lesion glycolysis; T2 volume, tumor volume on T2 series; T2 entropy, tumor entropy on T2 series; DWI volume, tumor volume on diffusion weighted imaging series; ADC mean, mean apparent diffusion coefficient; DWI entropy, tumor entropy on diffusion weighted imaging series; GLCM: grey level cooccurrence matrix, GLDM: grey level dependence matrix, GLRLM: grey level run length matrix, RI, response index (change over time).

Feature	Regression coefficient	Odds ratio	Standard error	95% confidence interval		P value
				Lower limit	Upper limit	
Baseline T2: tumor volume	0.999	2.716	0.584	0.864	8.537	0.087
Baseline T2: entropy	0.06	1.062	0.536	0.371	3.037	0.911
Baseline DWI: mean ADC	0.827	2.287	0.583	0.730	7.168	0.156
Baseline DWI: tumor volume	0.464	1.591	0.525	0.568	4.456	0.377
Baseline DWI: entropy	0.537	1.711	0.570	0.559	5.231	0.347
Baseline T2: grey level non-uniformity (GLDM)	-0.405	0.667	0.655	0.185	2.408	0.536
Baseline T2: grey level variance (GLDM)	0.195	1.216	0.531	0.429	3.445	0.713
Baseline DWI: difference entropy (GLCM)	-0.940	0.391	0.695	0.100	1.527	0.177
Baseline DWI: run length non-uniformity (GLRLM)	-0.360	0.697	0.598	0.216	2.250	0.546
Baseline PET: SUV <sub>max</sub>	0.210	1.233	0.520	0.445	3.418	0.687
Baseline PET: SUL <sub>peak</sub>	0.388	1.475	0.511	0.541	4.016	0.447
Baseline PET: MTV	0.764	2.147	0.552	0.728	6.337	0.166
Baseline PET: TLG	0.773	2.166	0.543	0.748	6.276	0.154
Early T2: tumor volume	0.220	1.246	0.517	0.452	3.435	0.670
Early T2: entropy	0.686	1.986	0.571	0.648	6.084	0.230
Early DWI: ADC mean	-0.003	0.997	0.536	0.349	2.848	0.995
Early DWI: tumor volume	-0.184	0.832	0.561	0.277	2.497	0.743
Early DWI: entropy	-0.376	0.687	0.571	0.224	2.104	0.511
Early T2: small dependence low grey level emphasis (GLDM)	-0.061	0.941	0.414	0.418	2.120	0.883
Early T2: joint entropy (GLCM)	-0.745	0.475	0.651	0.133	1.699	0.252
Early DWI: inverse difference (GLCM)	0.273	1.314	0.563	0.436	3.957	0.628
Early DWI: total energy (first order)	0.208	1.231	0.515	0.449	3.376	0.686
Early PET: SUV <sub>max</sub>	-1.159	0.314	1.061	0.039	2.508	0.274
Early PET: SUL <sub>peak</sub>	-0.778	0.459	0.916	0.076	2.764	0.396
Early PET: MTV	0.532	1.702	0.529	0.603	4.803	0.315
Early PET: TLG	0.001	1.001	0.535	0.351	2.856	0.999
Late T2: tumor volume	0.150	1.161	0.520	0.419	3.221	0.774
Late T2: entropy	-0.579	0.560	0.583	0.179	1.755	0.320
Late DWI: ADC mean	0.181	1.199	0.533	0.422	3.407	0.734
Late DWI: tumor volume	0.228	1.256	0.540	0.436	3.616	0.673
Late DWI: entropy	0.276	1.318	0.539	0.459	3.788	0.608

**TABLE 2. Continued.**

Feature	Regression coefficient	Odds ratio	Standard error	95% confidence interval		P value
				Lower limit	Upper limit	
Late T2: grey level non-uniformity (GLDM)	0.889	2.432	0.587	0.770	7.687	0.130
Late T2: joint entropy (GLCM)	-0.703	0.495	0.626	0.145	1.688	0.261
Late DWI: inverse difference normalized (GLCM)	-1.077	0.341	0.672	0.091	1.271	0.109
Late DWI: grey level non-uniformity normalized (GLRLM)	1.001	2.722	0.692	0.702	10.558	0.148
Late PET: SUV <sub>max</sub>	0.263	1.301	0.531	0.459	3.686	0.621
Late PET: SUL <sub>peak</sub>	0.631	1.880	0.575	0.610	5.800	0.272
Late PET: MTV	2.441	11.480	1.278	0.937	140.578	0.056
Late PET: TLG	5.499	244.488	4.385	0.045	1320336.926	0.210
Early – baseline T2: tumor volume RI	-1.781	0.168	1.179	0.017	1.699	0.131
Early – baseline T2: entropy RI	0.522	1.685	0.568	0.553	5.134	0.359
Early – baseline DWI: ADC mean RI	-0.923	0.397	0.673	0.106	1.486	0.170
Early – baseline DWI: tumor volume RI	-0.089	0.915	0.569	0.300	2.789	0.875
Early – baseline DWI: entropy RI	-0.860	0.423	0.721	0.103	1.738	0.233
Early – baseline PET: SUV <sub>max</sub> RI	-1.150	0.316	0.653	0.088	1.139	0.078
Early – baseline PET: SUL <sub>peak</sub> RI	-1.096	0.334	0.621	0.099	1.129	0.078
Early – baseline PET: MTV RI	0.434	1.543	0.518	0.559	4.259	0.402
Early – baseline PET: TLG RI	0.210	1.233	0.509	0.455	3.347	0.680
Late – baseline T2: tumor volume RI	-1.700	0.183	1.496	0.010	3.427	0.256
Late – baseline T2: entropy RI	-0.325	0.723	0.544	0.249	2.098	0.550
Late – baseline DWI: ADC mean RI	-0.480	0.619	0.626	0.182	2.110	0.443
Late – baseline DWI: tumor volume RI	-0.141	0.869	0.560	0.290	2.603	0.801
Late – baseline DWI: entropy RI	-0.198	0.821	0.575	0.266	2.533	0.731
Late – baseline PET: SUV <sub>max</sub> RI	0.410	1.507	0.522	0.541	4.197	0.432
Late – baseline PET: SUL <sub>peak</sub> RI	0.600	1.823	0.571	0.595	5.582	0.293
Late – baseline PET: MTV RI	0.523	1.687	0.520	0.609	4.676	0.315
Late – baseline PET: TLG RI	1.062	2.892	0.856	0.540	15.482	0.215

Abbreviations: SUV<sub>max</sub>, maximum standardized uptake value; SUL<sub>peak</sub>, peak standardized uptake value corrected for lean body mass; MTV, metabolic tumor volume; TLG, total lesion glycolysis; T2 volume, tumor volume on T2 series; T2 entropy, tumor entropy on T2 series; DWI volume, tumor volume on diffusion weighted imaging series; ADC mean, mean apparent diffusion coefficient; DWI entropy, tumor entropy on diffusion weighted imaging series; GLCM: grey level cooccurrence matrix, GLDM: grey level dependence matrix, GLRLM: grey level run length matrix, RI, response index (change over time).

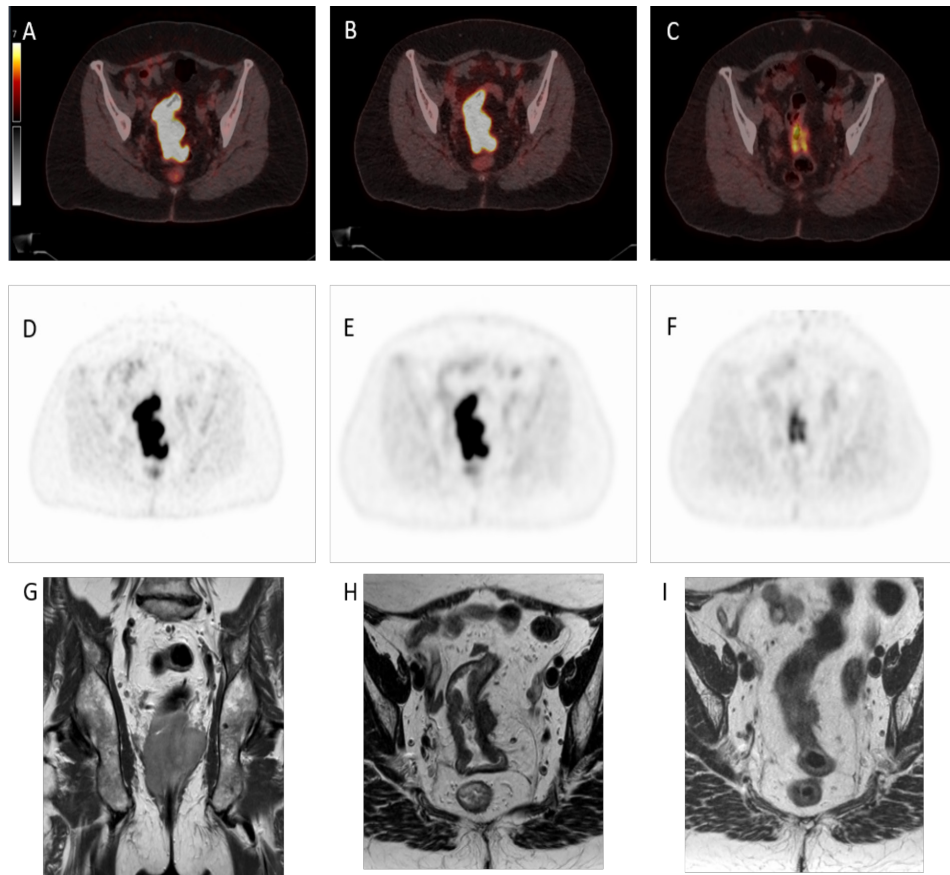


**FIGURE 2. [<sup>18</sup>F]FDG PET/CT and T2 weighted MRI images of a poor responder before, during and after neoadjuvant chemoradiotherapy.** Fifty-eight year old woman with cT4aN2M0 rectal cancer had a partial response to chemoradiotherapy to a yiT3N1M0. Pathological examination showed a ypT3N0M0 tumor and pTRG of 4. SUV<sub>max</sub> was 17.8 at baseline, 17.8 at interim assessment, and 6.5 at re-evaluation. Figure shows [<sup>18</sup>F]FDG PET/CT fusion (A, B, C) and PET-only (D, E, F) images as well as T2 weighted MRI (G, H, I) images before (A, D, G), during (B, E, H) and after (C, F, I) neoadjuvant chemoradiotherapy.

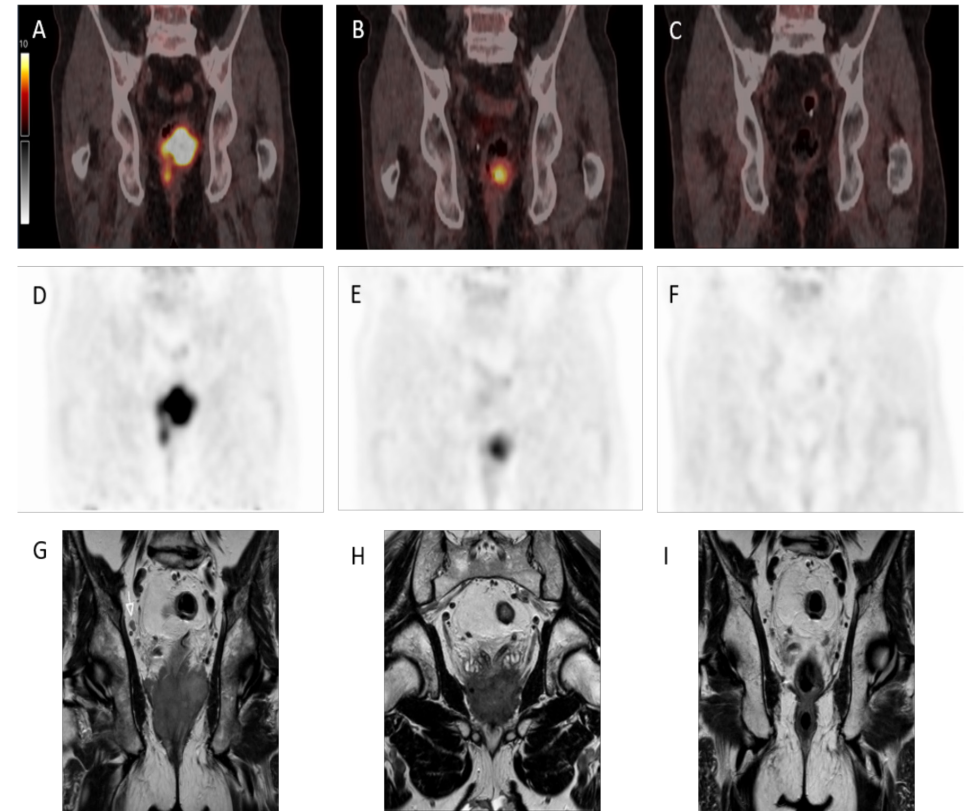


**FIGURE 3. [<sup>18</sup>F]FDG PET/CT and T2 weighted MRI images before, during and after neoadjuvant therapy of a patient with a clinical complete response.** Sixty-two year old man with cT4bN2M0 rectal cancer had a good response to a yiT1-2N0M0 which further regressed to a yiT0N0M0 six months after chemoradiotherapy, and is currently still followed in the Watch-and-Wait after 12 months of recurrence free follow up. SUV<sub>max</sub> was 18.1 at baseline, 10.4 at interim assessment, and too low to measure at re-evaluation. Figure shows [<sup>18</sup>F]FDG PET/CT fusion (A, B, C) and PET-only (D, E, F) images as well as T2 weighted MRI (G, H, I) images before (A, D, G), during (B, E, H) and after (C, F, I) neoadjuvant chemoradiotherapy.

## DISCUSSION

Results from this pilot study indicate that 13 out of 57 features are promising predictors of response, with baseline and early change showing the most clinically relevant features. As deduced from these results, end-of-treatment pre-surgical evaluation digital PET/CT was least probable to provide predictive (and clinically relevant) features. As far as we know, this is the first prospective study in LARC patients investigating the predictive value of multiparametric MRI and digital [<sup>18</sup>F]FDG PET/CT, at 3 set time points during neoadjuvant chemoradiation.

The results from this study confirm the feasibility of response prediction using digital [<sup>18</sup>F]FDG PET/CT and multiparametric MRI. These results are in line with previous reports from various small trials demonstrating the predictive value of various T2- and DW MRI and [<sup>18</sup>F]FDG PET/CT features, which have up until now not resulted in clinically usable prediction models<sup>14,17</sup>. In contrast to our results, a recent study in 19 LARC patients found only baseline MTV and no early response evaluation features (2 weeks into nCRT) to be possible predictors of response<sup>31</sup>. In our study we also found baseline MTV to be a promising feature. However, we also found 4 other baseline features (3 MRI, 1 PET) and 4 early response evaluation RI features (2 MRI, 2 PET). Interestingly, they found more predicting features at end-of-treatment pre-surgical evaluation [<sup>18</sup>F]FDG PET/CT (SUV<sub>max</sub>, SUV<sub>peak</sub>, MTV, SUL<sub>peak</sub>, TLG), whereas our study only found MTV to be a promising feature (note that the exact timing of the late evaluation [<sup>18</sup>F]FDG PET/CT in their study is unclear). As a next step towards clinical implementation, Schurink *et al.* developed prediction models including features from MRI and [<sup>18</sup>F]FDG PET/CT that were also used in the current study. The first study found an area under the curve (AUC) of 0.83 for response prediction at baseline using MRI derived T-stage, T2 entropy and T2 volume<sup>19</sup>. The second study found an AUC of 0.83 using clinical (T-stage, N-stage, age, gender, interval between nCRT and end-of-treatment pre-surgical evaluation) and baseline features (T2 entropy, ADC entropy and SUV<sub>mean</sub>)<sup>20</sup>. Interestingly, models including radiomic features did not outperform the simpler model<sup>20</sup>. Moreover, radiomic analysis of PET/CT images (AUC 0.78) did outperform simpler features (SUV<sub>mean</sub>, TLG and mean Hounsfield unit, AUC 0.50)<sup>20</sup>. However, PET/CT radiomic analyses were performed on the CT-only images, thus questioning the added value of PET. In comparison to our study, in which MRI-based radiomic features were analysed, we found 4 out of 12 radiomic features to be promising predictors of response (1 baseline and 3 end-of-treatment pre-surgical evaluation features). Unfortunately, no AUC values were available due to the limited number of patients. Interestingly, the end-of-treatment pre-surgical evaluation [<sup>18</sup>F]FDG PET/CT was least promising in this dataset. This might be due to the occurrence of radiation induced proctitis interfering with end-of-treatment pre-surgical evaluation PET/CT, since inflammation results in increased uptake of [<sup>18</sup>F]FDG and is not present at early response evaluation yet.

Although accurate response prediction is currently challenging, the significant number of unidentified complete responders who undergo surgical resection stresses the importance of accurate response assessment and prediction. Following our results, a future trial should include multiparametric MRI at all three timepoints, and [<sup>18</sup>F]FDG PET/CT at baseline and early response evaluation. Furthermore, the sample size should be sufficient to define cut-off values and develop accurate prediction models. While this study focused primarily on predicting response using imaging modalities, the (combined) use of readily available predictive features such as metabolomics and analysis of biopsy

material, and the integration of these in prediction models might further increase the accuracy of response prediction.

As inherent to any pilot study, this trial has various limitations. Due to the inclusion of only 19 patients and analysis of 57 features, no definite conclusions can be drawn from the data but only suggestions can be given towards design of future clinical trials. Due to the multicentric execution of this study various MRI scanners, with varying field strength, from various vendors and with varying scanning protocols were used. This introduces heterogeneity in the quantitative MRI features. Nevertheless, this reflects the clinical routine as the acquisition of a larger dataset of LARC patients requires inclusion from multiple hospitals. Preferably quantitative parameters would be compared from the various MRI scanners, protocols and field strengths. However, such a dataset is currently unavailable. A previous study by Mes *et al.*, however, found minimal influence of varying signal intensities from various MRI scanners on the outcome of radiomics analysis, thus suggesting the influence of this heterogeneity to be limited (high concordance (mean 0.82 ± 0.19) for 89 radiomics features before and after grey level normalization)<sup>32</sup>. Most recently, Schurink *et al.* investigated the influence of multiple MRI vendors and acquisition protocols on radiomic analysis in 649 rectal cancer patients<sup>33</sup>. They found significant differences in image features between 9 centres, with more differences found in ADC/DWI imaging compared to T2 weighted MRI. Last, inter observer variability has been introduced as the TRG was determined by various local pathologists. However, as the data were divided into only two groups, the influence of this was deemed minimal. Future studies should take these issues into account, and either further investigate the possible influence of various scanner types and acquisition protocols, perform the study on one MRI scanner within the same institute, or develop methods to harmonize the data. Also, a future study should consider the possible shift towards the use of more short course radiotherapy combined with systemic chemotherapy following results from the RAPIDO trial, as opposed to CRT as described by current guidelines<sup>3</sup>. This issue is less relevant for pooling data from [<sup>18</sup>F]FDG PET/CT, since data are (largely) harmonized by following the EANM guidelines and only one single PET/CT scanner was used in this study<sup>22</sup>.

In conclusion, results from this study suggest that baseline, early response and end-of-treatment pre-surgical evaluation MRI and baseline and early response evaluation PET/CT features are promising to predict response to neoadjuvant therapy in rectal cancer patients. These results, in combination with the clinical need for improved treatment stratification, encourage further research into response prediction using [<sup>18</sup>F]FDG PET/CT and multiparametric MRI.

## REFERENCES

1. Maas M, Nelemans PJ, Valentini V, et al. Long-term outcome in patients with a pathological complete response after chemoradiation for rectal cancer: a pooled analysis of individual patient data. *Lancet Oncol*. 2010;11:835–844.
2. Al-Sukhni E, Attwood K, Mattson DM, et al. Predictors of Pathologic Complete Response Following Neoadjuvant Chemoradiotherapy for Rectal Cancer. *Ann Surg Oncol*. 2016;23:1177–1186.
3. Bahadoer RR, Dijkstra EA, van Etten B, et al. Short-course radiotherapy followed by chemotherapy before total mesorectal excision (TME) versus preoperative chemoradiotherapy, TME, and optional adjuvant chemotherapy in locally advanced rectal cancer (RAPIDO): a randomised, open-label, phase 3 trial. *Lancet Oncol*. 2021;22:29–42.
4. Park J-S, Baek J-H, Lee W-S, et al. Long-term oncologic outcomes in pathologic tumor response after neoadjuvant chemoradiation for locally advanced rectal cancer. *Korean J Clin Oncol*. 2018;14:37–42.
5. Beets-Tan RGH, Lambregts DMJ, Maas M, et al. Magnetic resonance imaging for clinical management of rectal cancer: Updated recommendations from the 2016 European Society of Gastrointestinal and Abdominal Radiology (ESGAR) consensus meeting. *Eur Radiol*. 2018;28:1465–1475.
6. Landelijke Werkgroep Gastro Intestinale Tumoren. Oncoline Available from: <https://www.oncoline.nl/colorectaalcarcinoom>. Accessed November 6, 2019.
7. van der Valk MJM, Hilling DE, Bastiaannet E, et al. Long-term outcomes of clinical complete responders after neoadjuvant treatment for rectal cancer in the International Watch & Wait Database (IWWD): an international multicentre registry study. *Lancet Lond Engl*. 2018;391:2537–2545.
8. Hendren SK, O'Connor BI, Liu M, et al. Prevalence of male and female sexual dysfunction is high following surgery for rectal cancer. *Ann Surg*. 2005;242:212–223.
9. Dutch Guideline Colorectal Cancer. Federation Medical Specialists Available from: [https://richtlijnendatabase.nl/richtlijn/colorectaal\\_carcinoom\\_crc](https://richtlijnendatabase.nl/richtlijn/colorectaal_carcinoom_crc). 2019. Accessed December 25, 2021.
10. van Stiphout RGPM, Valentini V, Buijssen J, et al. Nomogram predicting response after chemoradiotherapy in rectal cancer using sequential PETCT imaging: a multicentric prospective study with external validation. *Radiother Oncol J Eur Soc Ther Radiol Oncol*. 2014;113:215–222.
11. Janssen MHM, Öllers MC, van Stiphout RGPM, et al. PET-based treatment response evaluation in rectal cancer: prediction and validation. *Int J Radiat Oncol Biol Phys*. 2012;82:871–876.
12. Cliffe H, Patel C, Prestwich R, et al. Radiotherapy response evaluation using FDG PET-CT—established and emerging applications. *Br J Radiol*.;90 . DOI: 10.1259/bjr.20160764.
13. Joye I, Debuquoy A, Deroose CM, et al. Quantitative imaging outperforms molecular markers when predicting response to chemoradiotherapy for rectal cancer. *Radiother Oncol J Eur Soc Ther Radiol Oncol*. 2017;124:104–109.
14. Mahadevan LS, Zhong J, Venkatesulu B, et al. Imaging predictors of treatment outcomes in rectal cancer: An overview. *Crit Rev Oncol Hematol*. 2018;129:153–162.
15. Meng X, Huang Z, Wang R, et al. Prediction of response to preoperative chemoradiotherapy in patients with locally advanced rectal cancer. *Biosci Trends*. 2014;8:11–23.
16. Giannini V, Mazzetti S, Bertotto I, et al. Predicting locally advanced rectal cancer response to neoadjuvant therapy with 18F-FDG PET and MRI radiomics features. *Eur J Nucl Med Mol Imaging*. 2019;46:878–888.
17. Joye I, Deroose CM, Vandecaveye V, et al. The role of diffusion-weighted MRI and (18)F-FDG PET/CT in the prediction of pathologic complete response after radiochemotherapy for rectal cancer: a systematic review. *Radiother Oncol J Eur Soc Ther Radiol Oncol*. 2014;113:158–165.
18. Avallone A, Aloj L, Pecori B, et al. 18F-FDG PET/CT Is an Early Predictor of Pathologic Tumor Response and Survival After Preoperative Radiochemotherapy with Bevacizumab in High-Risk Locally Advanced Rectal Cancer. *J Nucl Med Off Publ Soc Nucl Med*. 2019;60:1560–1568.
19. Schurink NW, Min LA, Berbee M, et al. Value of combined multiparametric MRI and FDG-PET/CT to identify well-responding rectal cancer patients before the start of neoadjuvant chemoradiation. *Eur Radiol*. 2020;30:2945–2954.
20. Schurink NW, van Kranen SR, Berbee M, et al. Studying local tumour heterogeneity on MRI and FDG-PET/CT to predict response to neoadjuvant chemoradiotherapy in rectal cancer. *Eur Radiol*. . Epub ahead of print February 10, 2021. DOI: 10.1007/s00330-021-07724-0.
21. Maffione AM, Marzola MC, Capirci C, et al. Value of (18)F-FDG PET for Predicting Response to Neoadjuvant Therapy in Rectal Cancer: Systematic Review and Meta-Analysis. *AJR Am J Roentgenol*. 2015;204:1261–1268.
22. Boellaard R, Delgado-Bolton R, Oyen WJG, et al. FDG PET/CT: EANM procedure guidelines for tumour imaging: version 2.0. *Eur J Nucl Med Mol Imaging*. 2015;42:328–354.
23. Kikinis R, Pieper SD, Vosburgh KG. 3D Slicer: A Platform for Subject-Specific Image Analysis, Visualization, and Clinical Support. In: Jolesz FA, ed. *Intraoperative Imaging and Image-Guided Therapy*. New York, NY: Springer;277–289.
24. van Griethuysen JJ, Fedorov A, Parmar C, et al. Computational Radiomics System to Decode the Radiographic Phenotype. *Cancer Res*. 2017;77:e104–e107.
25. Delli Pizzi A, Chiarelli AM, Chiacchiaretta P, et al. MRI-based clinical-radiomics model predicts tumor response before treatment in locally advanced rectal cancer. *Sci Rep*. 2021;11:5379.
26. van Timmeren JE, Cester D, Tanadini-Lang S, et al. Radiomics in medical imaging—“how-to” guide and critical reflection. *Insights Imaging*. 2020;11:91.
27. O JH, Lodge MA, Wahl RL. Practical PERCIST: A Simplified Guide to PET Response Criteria in Solid Tumors 1.0. *Radiology*. 2016;280:576–584.
28. Mandard AM, Dalibard F, Mandard JC, et al. Pathologic assessment of tumor regression after preoperative chemoradiotherapy of esophageal carcinoma. Clinicopathologic correlations. *Cancer*. 1994;73:2680–2686.
29. Peeters C, Übelhör C, Mes S, et al. Stable prediction with radiomics data. 2019.
30. Gillies RJ, Kinahan PE, Hricak H. Radiomics: Images Are More than Pictures, They Are Data. *Radiology*. 2016;278:563–577.
31. Uslu-Besli L, Mermut Ö, Yardimci AH, et al. Comparison of 18F-FDG PET/CT and DW-MRI in assessment of neoadjuvant radiochemotherapy response in locally advanced rectal cancer patients. *Rev Espanola Med Nucl E Imagen Mol*. 2021;40:19–29.
32. Mes SW, van Velden FHP, Peltenburg B, et al. Outcome prediction of head and neck squamous cell carcinoma by MRI radiomic signatures. *Eur Radiol*. 2020;30:6311–6321.

33. Schurink NW, van Kranen SR, Roberti S, et al. Sources of variation in multicenter rectal MRI data and their effect on radiomics feature reproducibility. *Eur Radiol.* 2022;32:1506–1516.

## SUPPLEMENTARY

**SUPPLEMENTAL TABLE 1. Specifications of MRI scanners.** Table shows specifications of various MRI scanners used in this study.

Vendor	Field strength (Tesla)	Number of scans	Acquisition voxel size (mm)
Philips Ingenia	1.5	6	0.62 x 0.81
Philips Ingenia	1.5	2	1.49 x 2.00
Philips Ingenia	1.5	15	0.49 x 0.64
Philips Ingenia	3	1	0.94 x 1.25
Philips Ingenia	3	1	0.49 x 0.62
Philips Ingenia	3	7	0.49 x 0.62
Philips Ingenia Elition X	3	9	0.70 x 0.79
Philips Ingenia Elition X	3	1	0.70 x 0.53
Philips Ingenia Elition X	3	1	0.89 x 1.56
Siemens Avanto	1.5	1	0.69 x 0.80
Siemens Avanto	1.5	1	0.63 x 0.73
Siemens Avanto	1.5	1	0.59 x 0.78
Siemens Avanto	1.5	1	0.47 x 0.67
Siemens Avanto	1.5	1	0.51 x 0.72
Siemens Avanto	1.5	1	0.63 x 0.79
Siemens Aera	1.5	2	0.47 x 0.59
Siemens Aera	1.5	6	0.63 x 0.78

MRI sequences included T2 weighted sequences in sagittal, oblique axial and oblique coronal direction and an orthogonal diffusion weighted imaging (DWI) sequence (*b*-values 0, 200, and 800/1000, identical direction of T2 oblique axial). Oblique axial scans were perpendicular to the long axis of the rectal wall.